coatings

MDPI

Article

Hydrophobic and Transparent Tantalum Pentoxide-Based Coatings for Photovoltaic (PV) Solar Panels

Oana Cătălina Mocioiu [1,*], Irina Atkinson [1], Ludmila Aricov [1], Veronica Bratan [1], Ana-Maria Mocioiu [2], Ioan Albert Tudor [2] and Diana Irinel Băilă [3]

[1] Institute of Physical Chemistry Ilie Murgulescu of the Romanian Academy—ICF, Splaiul Independentei, No. 202, 060021 Bucharest, Romania; iatkinson@icf.ro (I.A.); laricov@icf.ro (L.A.); vbratan@icf.ro (V.B.)
[2] National R&D Institute for Non-Ferrous and Rare Metals—IMNR, Biruintei Blv. 102, Pantelimon, 077145 Ilfov, Romania; ammocioiu@imnr.ro (A.-M.M.); atudor@imnr.ro (I.A.T.)
[3] Faculty of Industrial Engineering and Robotics, National University of Science and Technology Politehnica Bucharest—UPB, Splaiul Independentei, No. 313, 060042 Bucharest, Romania; baila_d@yahoo.com
* Correspondence: omocioiu@icf.ro

Abstract: Photovoltaic (PV) solar panels suffer from efficiency losses due to the accumulation of dust on their surface during operation, as well as the loss of transparency in the top glass. The efficiency can be increased when hydrophobic films are deposited on the top glass of the solar cells. The top glass of solar cells must have three characteristics: high transmittance in the 380–750 nm range, a band gap greater than 3.2 eV and a refractive index higher than 1.23. So, the films require the same characteristics. This work presents an increase in the contact angle (related to an increase in the hydrophobic character) when Ta_2O_5 is partially substituted with ZnO. The studied films, physically deposited on glass by e-gun technology, present a non-crystalline state in the form of the X-ray patterns shown. The films have a transmission of 75%–80% in the visible range. The morphology and roughness of the coatings were evaluated by atomic force microscopy. All films show the values of the Millipore water contact angle higher than 91 degrees, leading to the acquisition of hydrophobic properties on the surface. In comparison, the substrate is hydrophilic, with an average contact angle of 53.81 ± 2.16. The hydrophobic properties and self-cleaning ability make the films recommendable for application. The band gap of the coatings was calculated with the Tauc method, and they have values of 4.5–4.6 eV.

Keywords: hydrophobic; glass; e-gun technology; tantalum pentoxide; coatings

Citation: Mocioiu, O.C.; Atkinson, I.; Aricov, L.; Bratan, V.; Mocioiu, A.-M.; Tudor, I.A.; Băilă, D.I. Hydrophobic and Transparent Tantalum Pentoxide-Based Coatings for Photovoltaic (PV) Solar Panels. *Coatings* **2024**, *14*, 273. https://doi.org/10.3390/coatings14030273

Academic Editors: Rafael Comesaña and Feng Wang

Received: 6 November 2023
Revised: 28 December 2023
Accepted: 20 February 2024
Published: 23 February 2024

1. Introduction

Solar photovoltaic technology has developed rapidly in the last ten years due to its environmental friendliness and sustainability [1–8]. As global energy demand increases, the conversion of solar energy into electrical energy emerges as an alternative. There are different types of solar cells, but all of them have a top glass, also named glass superstrate, on the sun-facing side. The efficiency of solar cells is a problem due to the absorption of a part of solar energy. Worldwide, researchers are studying ways to increase cell efficiency.

The efficiency reported [4] for Si-based solar cells is between 10.2% in the case of Si (amorphous cell) and 26.7% for Si (multi-crystalline cells). Another type of PV panel is based on the perovskite solar cells [1–3]. The conversion efficiency of perovskite solar cells increased from 3.8% in 2009 to 28.75% in 2023 [5].

The photovoltaic solar panels' efficiency suffers due to the transparency and reflectance in the visible domain, as well as dust deposition from the atmosphere [6,8]. The deposition of dust on photovoltaic panels has become a big problem because it leads to a decrease in photovoltaic efficiency. Dust particles with diameters between 1 and 100 μm under the influence of gravity are deposited.

Mineral dust aerosols impact the radiation budget of earth through interactions with clouds, ecosystems and radiation, which constitutes a substantial uncertainty in understanding past climate changes and predicting future climate changes [9]. The fraction of emitted dust aerosols in the size range (<2 μm) interact most efficiently with shortwave (solar) radiation and have the longest lifetime [9].

The deposition of dust particles on outdoor panels may reduce the transmittance of solar cells and cause a significant decrease in the solar conversion efficiency of PV [10]. The performance of the panel is greatly influenced by environmental factors such as wind, temperature, humidity and dust [10]. The solar cell has a voltage drop of 27% and 28% power loss due to dust settling on it [10]. Rain cleans the PV panels in a temperate climate, but in an arid area, there is not enough precipitation and more dust [10]. Sharma [11] studied two types of solar photovoltaic panels located in the desert. One photovoltaic system was cleaned every two days, and the other one was never cleaned [11]. The results identified a decrease of 70% after 12 months of exposure due to the deposition of dust on the surface of the uncleaned photovoltaic panel compared with the cleaned one [11]. Kaldellis and Kapsali [12] reported the PV efficiency decreased by 26% after operation in the desert regions for four months due to dust deposition. The intense irradiation and long lighting period in the desert are advantages in the placement of photovoltaic panels [13]. The study of the effects of dust size and density on efficiency led to the conclusion that small-sized dust particles have higher influences on solar photovoltaic efficiency [13]. Vivar's [14] results on the influence of wind on dust deposition showed that the growth of the airflow velocity led to higher deposition density.

In the literature are presented different methods that can be used for the self-cleaning of photovoltaic panels: the electrostatic method, mechanical method, hydrophobic method and hydrophilic methods [6,8].

This work studies the possibility of increasing the efficiency of solar cells when hydrophobic films are deposited on their top glass.

Lotus leaf is the first botanical surface that inspired the study of hydrophobic properties from a different perspective [15,16]. Hydrophobic lotus leaf presents self-cleaning properties due to a high-water contact angle of 150 degrees [15]. Lotus leaves become a symbol of hydrophobicity and self-cleaning surfaces, known as the 'lotus effect' [17]. The hydrophobicity and self-cleaning of lotus leaves are induced by a roughness given by micro- and nanoscale structures [16]. The structural properties, such as multiscale roughness, the physical property of the high repellence of the liquid droplets from the surface, and chemical properties are characteristics of the lotus leaves. The roughness is important for hydrophobic properties, as was presented by Kim [16]. When water droplets are attached to the lotus leaf surface, air pockets exist between the water droplets and the micro- and nanostructures, and this phenomenon is said to be in the Cassie–Baxter state [16]. According to the lotus effect and their self-cleaning property, liquid droplets or droplets containing dust on the lotus leaf surface roll off from the surface due to hydrophobicity [16]. The nanoscale tubules on the lotus leaf surface have an average height of 100–500 nm and a diameter of 100–300 nm [16].

The literature data reported thin films obtained by various methods [17–26]. The implementation of light management textures in thin film solar cells often simultaneously causes an unwanted deterioration of electronic performance [27–29]. A simple but effective technique for improving light absorption in thin-film solar cells consists of printing pyramidal textures on the sun-facing side of the glass superstrate [27]. Thus, the absorbent layer and the functional ones of the device remain unaffected while the light coupling is significantly increased [27]. An increase in short-circuit current density of 2.5 mA cm^2 was observed, corresponding to an increase in efficiency from 12.9% to 13.8% [27]. Imprinting a light management layer of random pyramids on top of perovskite/silicon tandem solar cells allowed for increasing the short-circuit current density in these devices by more than 1 mA cm^{-2}, resulting in a power conversion efficiency of 25.5% [27].

Lai reported a hydrophobic coating of ZnO/SiO_2 nanorods and sub-microtubes obtained by the hydrothermal combined with the sol–gel method [25].

Baxevani [17] studied the effect of roughness on the superhydrophobic silver foil on copper foam for good oil/water separation. The resulting coated foams exhibited water contact angles of 180° [17]. Separation efficiency was maintained at 94% for different pollutants, suggesting good stability and durability with no respect to roughness [17]. Fern [30] showed the CoFeSm film thickness increased, decreasing the crystalline size and surface roughness. The surface roughness of the Co-Fe-Sm films plays a crucial role in shaping the magnetic properties of these thin magnetic films [30].

ZnO or Ta_2O_5 films attracted the attention of researchers due to the possibility of obtaining various morphologies, such as nanorods or nanospheres, as well as good optical properties. Ta_2O_5 (3.97 eV) and ZnO (3.26 eV) TCOs, with their favorable attributes, including non-toxicity, cost-effectiveness, ease of preparation and robust optoelectronic properties, hold promise as suitable alternatives [19,23,24]. ZnO-doped tantalum oxide films (doping 1–5 wt.%) were prepared by the pulsed laser deposition technique in a reactive oxygen atmosphere, and the films were annealed at temperatures of 973 and 1173 K [31]. An XRD analysis shows that the ZnO-doped films annealed at 973 K are crystalline, whereas the annealed counterpart of pure Ta_2O_5 is amorphous. Upon annealing at 1173 K, the undoped film showed good crystallinity, whereas the ZnO-doped film presented a decline in crystallinity compared to that of the films annealed at 973 K [31]. The AFM photos of 3 and 5 wt.% ZnO-doped Ta_2O_5 films presented Ta_2O_5 nanoring with a diameter of 700 nm [31]. The band gap increases with ZnO doping and with the temperature of treatment. Deo [2] studied amorphous tantalum oxide (Ta_2O_5) deposited by spin coating as an electron transport material for perovskite solar cells, achieving power conversion efficiency up to ~14%. Amorphous Ta_2O_5 films can be the electron transporters in perovskite cells due to tantalum oxide as an n-type semiconductor with a calculated carrier density of $\sim 7 \times 10^{18}/cm^3$ [2]. Ta_2O_5 can be a possibility for optical devices due to its high refractive index in the visible domain, band gap proper for solar cells and high dielectric constant [32]. Ta_2O_5 film has prospective applications in devices such as optical filters, optical waveguides, non-linear optical devices and photonic crystals [32]. Ta_2O_5 thin films were obtained by pulsed laser ablation, magnetron sputtering, atomic layer deposition, ion beam sputtering and heat evaporation [32,33]. The synthesis of the Ta_2O_5 coatings with better properties requires the characterization of the coatings related to the preparation method. Among the deposition techniques, the e-beam deposition technique offers advantages compared with the other vapor deposition techniques, such as film uniformity and optical efficiency [34]. This control on film synthesis led to the possibility of designing the microstructure and composition as well as the properties.

Previously studied hydrophobic films showed crystalline structures, which means thermal treatments at high temperatures and implicit energy consumption [17,25,30]. The aim of this work is to develop non-crystalline coatings of the Ta_2O_5-ZnO type with hydrophobic (and implicitly self-cleaning) properties in order to increase the efficiency of photovoltaic solar panels over time. The coverings must absorb as little sunlight as possible (T > 70%) and have a reflection index according to the application.

2. Materials and Methods

Tantalum pentoxide coatings were deposited by e-gun technology on the borosilicate glass substrate. Zinc oxide, CAS No. 1314-13-2, from Sigma-Aldrich (St. Louis, MO, USA) and tantalum (V) oxide with purity 99%, CAS No. 1314-61-0, from Sigma-Aldrich (St. Louis, MO, USA) were used as raw materials. The coating deposition is similar to references [18,33]. The e-gun process was realized in a physical vapor deposition chamber; in high vacuum at pressure of 10^{-5} to 10^{-6} torr. Coating growth, thickness and evaporating rate were controlled by a quartz crystal microbalance. The compositions of the three coatings are Ta_2O_5 (100%), Ta_2O_5 (75%) and ZnO (25%), Ta_2O_5 (50%) and ZnO (50%). Both oxides were deposited simultaneously using a Z-550-S Leybold–Heraeus

(Cologne, Germany) sputtering system. The thickness of the coatings was controlled by own apparatus software, and it was established at 100 nm.

Both oxides were deposited simultaneously. The thickness of the coatings was controlled by apparatus, and it was established at 100 nm.

X-ray diffraction (XRD). The structure of the glass substrate and coatings deposited on the substrate were determined from patterns recorded with Ultima IV X-ray Diffractometer (Rigaku, Tokyo, Japan) and Cu Kα radiation.

FTIR spectroscopy was used to identify the bonds formed into coatings. The spectra of the coatings were recorded with a Nicolet 6700 spectrometer (Thermo Fisher Scientific, MA, USA) in the 400–1400 cm^{-1} range.

Atomic force microscopy (AFM). The surface morphology and roughness of coatings were investigated using a Nanovea microscope, model Nanosurf Nanite B (MA, USA), 110 microns. The measurements were performed in air at room temperature using contact mode and static force operation mode.

Easy Drop Shape Analyzer (DSA1, KRÜSS GmbH, Hamburg, Germany) was used to measure the contact angle of Millipore water on the prepared films at 24 °C in air. The samples were placed on a flat support, and the ultra-pure water was dropped using a stainless-steel needle (outer diameter of 0.5 mm). The drop volume was 3 μL. The contact angle was calculated using the sessile drop method. The measurements were repeated 6 times for each sample.

The optical properties were investigated by UV-VIS spectroscopy. The measurements were made in transmission mode using an Agilent Cary 100 spectrophotometer (Agilent Technologies Australia). The measurements were carried out in the 800–200 nm range. To eliminate the contribution of the glass substrate to the light absorption, the spectra were recorded using it as a reference. The transmittance data were processed for bandgap and refractive index calculations.

3. Results

Three coatings were obtained by e-gun technology and are presented in this article. The first coating, named Ta_2O_5, obtained from pure tantalum pentoxide, was a lilac color; the second coating, named $75Ta_2O_5$-25ZnO, was a magenta color and the third coating with half zinc oxide and half tantalum pentoxide, named $50Ta_2O_5$-50ZnO, was gray. The structural characterization of the coatings was carried out with X-ray diffraction (XRD) and infrared spectroscopy (FTIR). The morphologies and the roughness of the films were visualized by atomic force microscope. The contact angle was determined in order to establish the hydrophobic behavior of the coatings.

3.1. X-ray Diffraction (XRD)

Figure 1 shows the patterns of the coatings and the substrate glass. Ta_2O_5-based coatings have a non-crystalline state, and for this reason, they have no diffraction peaks. The sputtering power has little effect on the microstructure of the coatings, as shown by all the XRD spectra. Similar results were reported for Ta_2O_5 thin films in the literature [25]. However, two broad bands can be observed in the case of Ta_2O_5 and $75Ta_2O_5$-25ZnO coatings; related to a small nucleation of the tantalum pentoxide.

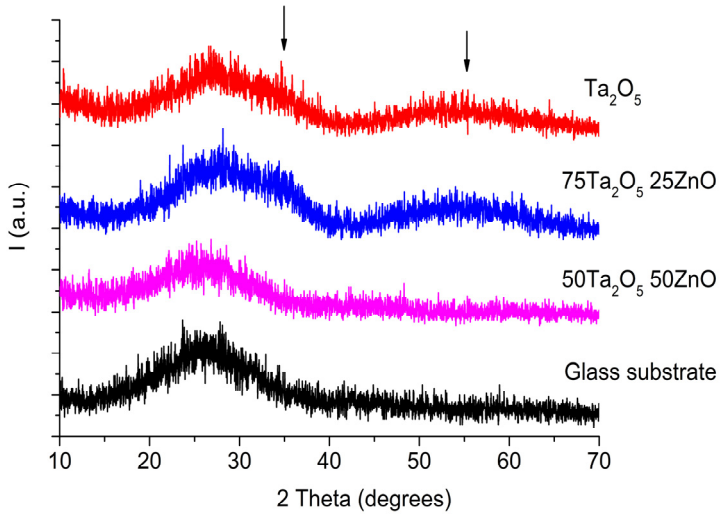

Figure 1. XRD patterns of the glass substrate and obtained coatings. The arrows show the place of the tantalum pentoxide peaks in crystal. In this case small and wide band can be assign to few structural units arrangement in non-crystalline film.

3.2. Infrared Spectroscopy (FTIR)

Infrared spectroscopy was used as a technique to identify the bonds present in the coatings. FTIR spectra for non-crystalline materials are different from the spectra of the crystalline materials. In crystalline materials, because there is an order in the lattice, several vibration bands for the same bond appear in the FTIR spectrum. The typical absorption bands of zinc oxide crystalline lattice were reported at 530 cm^{-1}, 495 cm^{-1}, 440 cm^{-1} and 677 cm^{-1} [32,34]. The FTIR bands of Zn-O- can be shifted to lower wavenumbers (420 cm^{-1}) in compounds such as zinc–stannate [34]. In the FTIR spectra of amorphous tantalum oxide films, in the 800–1000 cm^{-1} range, Ta–O–Ta stretching vibrations were reported [31]. The bands in the 400–800 cm^{-1} region were assigned to Ta–O–Ta and Ta–O- stretching modes [31]. In the spectrum of amorphous tantalum oxide films, the band at 452 cm^{-1} appears due to O–Ta–O bending vibrations in TaO_6 octahedra [31]. Krishnan [31] reported that amorphous and crystalline Ta_2O_5 was proposed as an ionic–covalent compound consisting of TaO_n^{5-2n} and $Ta_6O_{12}^{6+}$ clusters.

Figure 2 presents the FTIR spectra of pure Ta_2O_5 coating and $75Ta_2O_5$ 25ZnO coating. FTIR spectrum of Ta_2O_5 coating shows broad bands with no well-defined shape in the 1600–400 cm^{-1} domain, characteristic of an amorphous state. In the FTIR spectrum of $75Ta_2O_5$ 25ZnO film, the main bands can be observed at 430 cm^{-1}, 459 cm^{-1}, 468 cm^{-1}, 492 cm^{-1}, 556 cm^{-1}, 645 cm^{-1}, 706 cm^{-1}, 790 cm^{-1} and 857 cm^{-1}. In the spectrum of $75Ta_2O_5$ 25ZnO coating, the bands at 430 cm^{-1}, 492 cm^{-1} and 556 cm^{-1} could be assigned to the formation of Ta–O–Zn covalent bonds, and the bands at 459 cm^{-1}, 468 cm^{-1}, 645 cm^{-1}, 706 cm^{-1}, 790 cm^{-1} and 857 cm^{-1} are attributed to Ta–O–Ta and Ta–O stretching vibrations. The shape of the bands shows that the addition of zinc oxide led to a structuration of the lattice. This behavior was expected because zinc oxide acts as a network former in glasses. However, the ordering of the crystalline lattice occurs only at a few structural units. This is shown by the width of the bands in the spectrum.

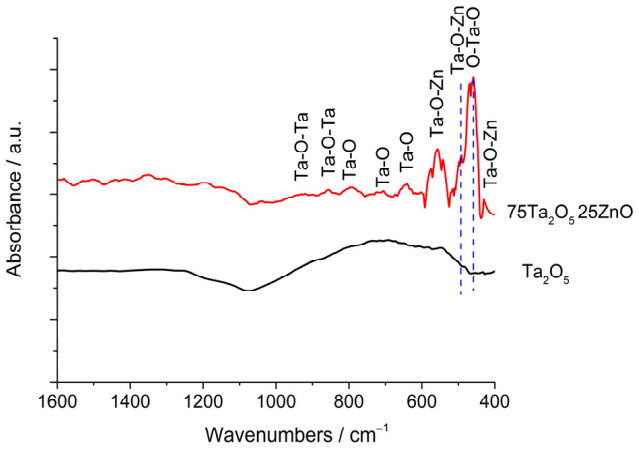

Figure 2. FTIR spectra of two obtained coatings (recorded with air as reference).

3.3. Atomic Force Microscopy (AFM)

Atomic force microscopy measurements were performed to evaluate the morphology and the roughness of the coatings. Table 1 shows the values of average roughness (Ra) and root mean square (Rrms) roughness of the studied films. The root mean square (Rrms) roughness, commonly used in AFM description, represents the standard deviation of the height value in the selected region. In the Supplementary Materials, the 2D and 3D images of the studied films are shown (Figure S1).

Table 1. The roughness parameters obtained by AFM.

Film	Roughness Parameters	
	Ra (nm)	**Rrms (nm)**
Ta_2O_5	2.82	3.31
75Ta_2O_5-25ZnO	4.86	5.63
50Ta_2O_5-50ZnO	7.04	9.7

The studied films have uniform coverage of the glass surface and different roughness. The roughness determined by AFM led to the following conclusions: (1) in the case of coatings with both oxides, a big addition of zinc oxide causes a higher roughness, and (2) the pure tantalum pentoxide coating presents a lower roughness.

3.4. Contact Angle (CA)

In Table 2, the results of contact angle measurements for substrate and coatings are presented. Table 2 includes the average CA and the mean deviation values for the three films. Dust deposition on the PV is highly influenced by water bonded to the glass surface [27–29]. If the glass surface is hydrophobic, the quantity of water remaining on the surface is lower, and the dust cannot adhere to the surface. One criterion to archive the self-cleaning and hydrophobic properties is the value of the water contact angle. The value of contact angle (CA) establishes surface properties such as hydrophobicity when CA > 90° or hydrophilicity when CA < 90° [6]. More theoretical details concerning the correlation between obtained roughness and hydrophobicity (contact angle) are presented in reference [6]. The contact angles of the studied films are in the 93.91 ± 1.83 and 110.66 ± 1.21 degree range, and all of them show hydrophobic properties. The contact angle of the glass substrate is between 50 and 54.5 degrees, so it is hydrophilic because it is below 90 degrees. It may be considered that the contact angle of the substrate did not influence the hydrophobic properties of deposited films. The presence of both oxides in the film composition has a good influence on the hydrophobic properties. The greatest hydrophobic coating has a composition of 75% Ta_2O_5 and 25% ZnO.

Table 2. Contact angle measurements for glass substrate and Ta_2O_5-based coatings.

Sample	The Average CA and the Mean Deviation Values	Image/Contact Angle (°)			
Glass Substrate	53.81 ± 2.16	 52.97	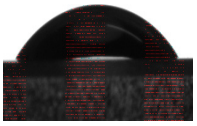 50.55	 58.16	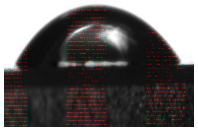 51.15
		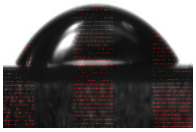 51.93	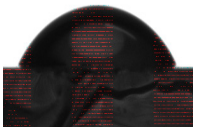 57.05	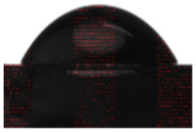 54.23	 54.50
Ta_2O_5	93.91 ± 1.83	 96.85	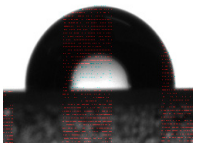 93.52	 93.92	 91.21
		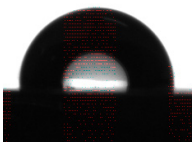 97.73	 92.14	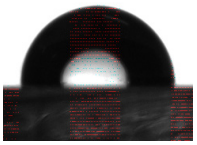 91.45	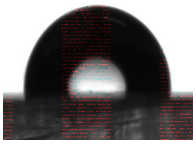 94.45
$75Ta_2O_5$ 25ZnO	111.05 ± 2.92	 114.89	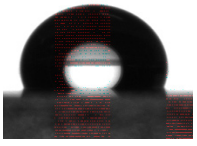 109.17	 114.94	 112.85
		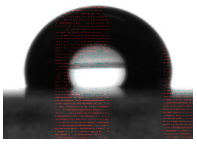 104.34	 108.44	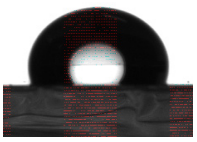 110.58	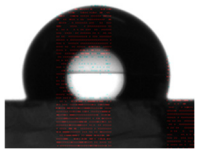 113.22
$50Ta_2O_5$ 50ZnO	110.66 ± 1.21	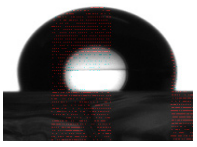 108.99	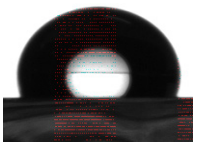 110.86	 108.92	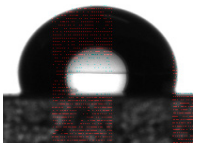 110.11
		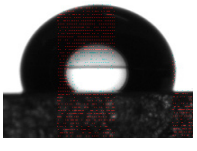 112.35	 112.69	 111.58	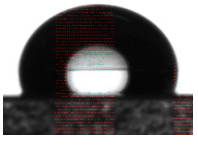 109.79

3.5. UV-VIS Spectroscopy

Figure 3 shows the experimental transmission spectra in the ultraviolet and visible range for studied films. The band gap and refractive index were determined using data from the UV-VIS spectra. Two different regions were observed in the pattern of the UV-VIS

spectra. The transparency region is located at a wavelength higher than ~330 nm, and its characteristic is low light absorption. In the transparency region (330–1000 nm), the average optical transmittance of Ta_2O_5 and $75Ta_2O_5$-25ZnO coatings is about 80% and decreases to 75% for the $50Ta_2O_5$-50ZnO coating. It seems that this last film is opaque, hence its gray color. Even though the transmittance decreased, it is still high enough to provide good efficiency for the solar cells. The optical loss decreased a little, but if dust settles on the solar cells, the optical loss will increase much more. Interference fringes in transmission spectra occur because the incident light moves between two interfaces (air–coating, coating–substrate), producing different reflected and transmitted waves that constructively or destructively interfere within the samples. The presence of these interference fringes indicates that the coatings have optically smooth surfaces, both with the air and with the substrate, and very good thickness homogeneity [35–37]. The deposited coating of $50Ta_2O_5$-50ZnO has lower transmittance as well as a small number of fringes. This could be related to its higher roughness, which results in much scattering of light over the coating's surface [35]. In the second region ($\lambda < 330$ nm), there is a sharp drop in optical transmission. This decrease can be attributed to inter-band transitions from the valence band to the conduction band for Ta_2O_5 and/or ZnO [32,37].

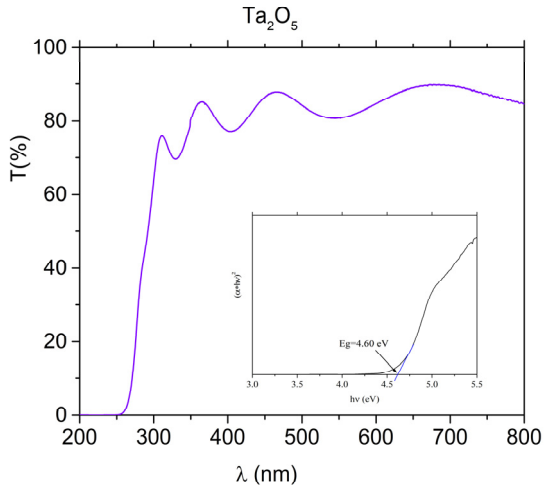

(**a**)

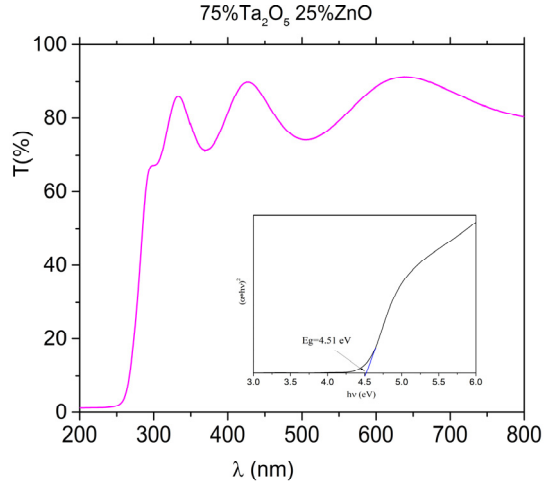

(**b**)

Figure 3. *Cont.*

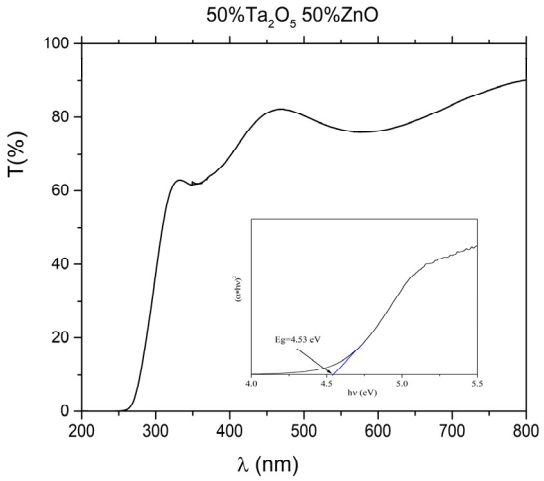

(**c**)

Figure 3. Transmission in UV-VIS domain for (**a**) Ta_2O_5 film; (**b**) $75Ta_2O_5$-25ZnO film; (**c**) $50Ta_2O_5$-50ZnO film. The reference used for the spectra registration was uncoated substrate.

The optical bandgap was calculated using the Tauc method [38], namely from a graphical representation of $[\alpha^*h\nu]^{1/\eta}$ vs. hν, where α is the absorption coefficient, h is the Planck constant, ν is the photon's frequency and η is a parameter whose value depends on the type of electron transitions (½ or 2, for direct or indirect transitions, respectively). The band gap is equal to the x-intercept when the linear region of the plot is extrapolated to zero.

The band gaps of the current films were determined considering direct transitions (insets in Figure S1a–c) and the obtained values were listed in Table 3. The optical band gap value for Ta_2O_5 is consistent with the direct band gap energies of the Ta_2O_5 films obtained by Chen [32]. The optical absorption energies were influenced by the ZnO content. The refractive index of a material is an important macroscopic parameter useful in the optoelectronic field. It is a function of many factors, such as energy, dopants or thickness. To minimize these influences, only the static/optical refractive index (due to the time-independent component of light and electric field) could be used [39]. Various relations were proposed in order to correlate the optical refractive index of a material to its band gap energy. In this study, we used the relationship (1) proposed by Ravindra [40] to determine the refractive index:

$$n = 4.08 - 0.62E_g \quad (1)$$

where n is the refractive index of the material, and E_g is the optical band gap.

Table 3. Band gap and refractive index of the coatings and glass substrate.

Sample	Eg (eV)	n
Ta_2O_5	4.6	1.23
$75Ta_2O_5$-25ZnO	4.51	1.28
$50Ta_2O_5$-50ZnO	4.53	1.27

This method was chosen because it provided a better match between the calculated refractive index of the substrate and its value listed in the Schott Company technical specifications. The band gap and the refractive index were correlated with the zinc oxide amount in the film. The good effect of zinc oxide can be observed in the properties of other nanomaterials and glasses used as semiconductors [34,41].

4. Conclusions

The transparent films were obtained by e-gun technology. In this work, an increase in the contact angle above 93 degrees (related to an increase in hydrophobicity) was reported when the composition of the Ta_2O_5 films was partially changed to ZnO. The addition of ZnO has a good influence on the properties. The best properties are obtained for the film with a composition of 75% Ta_2O_5 and 25% ZnO, a contact angle of 111.05° ± 2.92, a band gap of 4.51 eV and a refractive index of 1.28. The research has an applied value because it solves the problem of dust particle deposition on the sun-facing surface of photovoltaic cells. The studied films can be deposited on the top glass surface of solar cells to provide self-cleaning properties. The method reduces film production costs by eliminating an energy-consuming heat treatment step that can lead to film crystallization.

Supplementary Materials: The following supporting information can be downloaded at: https://www.mdpi.com/article/10.3390/coatings14030273/s1, Figure S1. Atomic Force Microscopy: 2D images (a,c,e) and 3D view (b,d,f); Ta_2O_5 film (a,b); $75Ta_2O_5$ 25ZnO film (c,d); $50Ta_2O_5$ 50ZnO film (e,f).

Author Contributions: Conceptualization, O.C.M.; obtaining methodology, D.I.B.; formal analysis, O.C.M., I.A., L.A., V.B., I.A.T. and A.-M.M., writing—original draft preparation, O.C.M. All authors have read and agreed to the published version of the manuscript.

Funding: This research was funded Program 4: Materials Science and Advanced Characterization Methods, Theme: 4.10.28 Synthesis and characterization of glassy and crystalline materials for solar cells and nanofluids, from "Ilie Murgulescu" Institute of Physical Chemistry of the Romanian Academy—ICF.

Institutional Review Board Statement: Not applicable.

Informed Consent Statement: Not applicable.

Data Availability Statement: Data are contained within the article and Supplementary Materials.

Conflicts of Interest: The authors declare no conflicts of interest.

References

1. Ma, Q.; Zhang, Y.; Lu, C.; Zhang, R.; Wang, X.; Zhang, W.; Jiang, Z. MACl-Induced Controlled Crystallization in Sequentially Deposited Perovskites for High-Efficiency and Stable Perovskite Solar Cells. *Coatings* **2023**, *13*, 1885. [CrossRef]
2. Deo, M.; Möllmann, A.; Haddad, J.; Ünlü, F.; Kulkarni, A.; Liu, M.; Tachibana, Y.; Stadler, D.; Bhardwaj, A.; Ludwig, T.; et al. Tantalum Oxide as an Efficient Alternative Electron Transporting Layer for Perovskite Solar Cells. *Nanomaterials* **2022**, *12*, 780. [CrossRef] [PubMed]
3. Arayro, J.; Mezher, R.; Sabbah, H. Comparative Simulation Study of the Performance of Conventional and Inverted Hybrid Tin-Based Perovskite Solar Cells. *Coatings* **2023**, *13*, 1258. [CrossRef]
4. Green, M.A.; Hishikawa, Y.; Dunlop, E.D.; Levi, D.H.; Hohl-Ebinger, J.; Ho-Baillie, A.W.Y. Solar cell efficiency tables. *Prog. Photovolt. Res. Appl.* **2018**, *26*, 3–12. [CrossRef]
5. Gan, Y.; Qiu, G.; Yan, C.; Zeng, Z.; Qin, B.; Bi, X.; Liu, Y. Numerical Analysis on the Effect of the Conduction Band Offset in Dion–Jacobson Perovskite Solar Cells. *Energies* **2023**, *16*, 7889. [CrossRef]
6. Syafiqa, A.; Pandeya, A.K.; Adzmana, N.N. Nasrudin Abd Rahim Superhydrophilic Smart Coating for Self-Cleaning Application on Glass Substrate. *Sol. Energy* **2018**, *162*, 597.
7. Suchikova, Y.; Kovachov, S.; Bohdanov, I.; Kozlovskiy, A.L.; Zdorovets, M.V.; Popov, A.I. Improvement of β-SiC Synthesis Technology on Silicon Substrate. *Technologies* **2023**, *11*, 152. [CrossRef]
8. Kudriavtsev, Y.; Hernandez, A.G.; Asomoza, R. Solar cell degradation caused by glass superstrate corrosion. *Sol. Energy* **2019**, *187*, 82–84. [CrossRef]
9. Kok, J.F. A scaling theory for the size distribution of emitted dust aerosols suggests climate models underestimate the size of the global dust cycle. *Proc. Natl. Acad. Sci. USA* **2011**, *108*, 1016–1021. [CrossRef] [PubMed]
10. Yadav, A.; Pillai, S.R.; Singh, N.; Philip, S.A.; Mohanan, V. Preliminary investigation of dust deposition on solar cells. *Mater. Today Proc.* **2021**, *46*, 6812–6815. [CrossRef]
11. Sharma, V.; Chandel, S.S. Performance and degradation analysis for long term reliability of solar photovoltaic systems: A review. *Renew. Sustain. Energy Rev.* **2013**, *27*, 753–767. [CrossRef]
12. Kaldellis, J.K.; Kapsali, M. Simulating the dust effect on the energy performance of photovoltaic generators based on experimental measurements. *Energy* **2011**, *36*, 5154–5161. [CrossRef]

13. Nugroho, H.S.; Refantero, G.; Septiani, N.L.W.; Iqbal, M.; Marno, S.; Abdullah, H.; Prima, E.C.; Nugraha; Yuliarto, B. A progress review on the modification of CZTS(e)-based thin-film solar cells. *J. Ind. Eng. Chem.* **2022**, *105*, 83. [CrossRef]
14. Vivar, M.; Herrero, R.; Anton, I.; Martinez-Moreno, F.; Moreton, R.; Sala, G.; Blakers, A.W.; Smeltink, J. Effect of soiling in CPV systems. *Sol. Energy* **2010**, *84*, 1327–1335. [CrossRef]
15. Ensikat, H.J.; Ditsche-Kuru, P.; Neinhuis, C.; Barthlott, W. Superhydrophobicity in perfection: The outstanding properties of the lotus leaf. *Beilstein J. Nanotechnol.* **2011**, *2*, 152–161. [CrossRef]
16. Kim, W.; Kim, D.; Park, S.; Lee, D.; Hyun, H.; Kim, J. Engineering lotus leaf-inspired micro- and nanostructures for the manipulation of functional engineering platforms. *J. Ind. Eng. Chem.* **2018**, *61*, 39–52. [CrossRef]
17. Baxevani, A.; Stergioudi, F.; Skolianos, S. The Roughness Effect on the Preparation of Durable Superhydrophobic Silver-Coated Copper Foam for Efficient Oil/Water Separation. *Coatings* **2023**, *13*, 1851. [CrossRef]
18. Mocioiu, A.-M.; Baila, D.-I.; Codrea, C.I.; Mocioiu, O.C. A Simple Method to Obtain Protective Film against Acid Rain. *Inorganics* **2022**, *10*, 44. [CrossRef]
19. Seyhan, A.; Kartal, E. Optical, Electrical and Structural Properties of ITO/IZO and IZO/ITO Multilayer Transparent Conductive Oxide Films Deposited via Radiofrequency Magnetron Sputtering. *Coatings* **2023**, *13*, 1719. [CrossRef]
20. Chen, T.-H.; Jian, B.-L. Optical and Electronic Properties of Mo:ZnO Thin Films Deposited Using RF Magnetron Sputtering with Different Process Parameters. *Opt. Quant. Electron.* **2016**, *48*, 77. [CrossRef]
21. Ponja, S.D.; Sathasivam, S.; Parkin, I.P.; Carmalt, C.J. Highly Conductive and Transparent Gallium Doped Zinc Oxide Thin Films via Chemical Vapor Deposition. *Sci. Rep.* **2020**, *10*, 638. [CrossRef]
22. Fu, Y.-C.; Chen, Y.-C.; Wu, C.-M.; Hsiao, V.K.S. Tailored Nanoscale Architectures for White Light Photoelectrochemistry: Zinc Oxide Nanorod-Based Copper Oxide Heterostructures. *Coatings* **2023**, *13*, 2051. [CrossRef]
23. Luo, Y.-T.; Zhou, Z.; Wu, C.-Y.; Chiu, L.-C.; Juang, J.-Y. Analysis of Hazy Ga- and Zr-Co-Doped Zinc Oxide Films Prepared with Atmospheric Pressure Plasma Jet Systems. *Nanomaterials* **2023**, *13*, 2691. [CrossRef]
24. Ellmer, K. Past Achievements and Future Challenges in the Development of Optically Transparent Electrodes. *Nat. Photonics* **2012**, *6*, 809. [CrossRef]
25. Lai, D.; Kong, G.; Che, C. Synthesis and corrosion behavior of ZnO/SiO_2 nanorod-sub microtube superhydrophobic coating on zinc substrate. *Surf. Coat. Technol.* **2017**, *315*, 509–518. [CrossRef]
26. Poortmans, J.; Arkhipov, V. *Thin Film Solar Cells*; John Wiley & Sons, Ltd.: Hoboken, NJ, USA, 2006.
27. Eisenhauer, D.; Trinh, C.T.; Amkreutz, D.; Becker, C. Light management in crystalline silicon thin-film solar cells with imprint-textured glass superstrate. *Sol. Energy Mater. Sol. Cells* **2019**, *200*, 109928. [CrossRef]
28. Quan, Z.; Lu, H.; Zhao, W.; Zheng, C.; Zhu, Z.; Qin, J.; Yue, M. A Review of Dust Deposition Mechanism and Self-Cleaning Methods for Solar Photovoltaic Modules. *Coatings* **2023**, *13*, 49. [CrossRef]
29. Ndeto, M.P.; Wekesa, D.W.; Njoka, F.; Kinyua, R. Correlating dust deposits with wind speeds and relative humidity to overall performance of crystalline silicon solar cells: An experimental study of Machakos County, Kenya. *Sol. Energy* **2022**, *246*, 203–215. [CrossRef]
30. Fern, C.-L.; Liu, W.-J.; Chang, Y.-H.; Chiang, C.-C.; Lai, J.-X.; Chen, Y.-T.; Chen, W.-G.; Wu, T.-H.; Lin, S.-H.; Lin, K.-W. Studying the Crucial Physical Characteristics Related to Surface Roughness and Magnetic Domain Structure in CoFeSm Thin Films. *Coatings* **2023**, *13*, 1961. [CrossRef]
31. Krishnan, R.R.; Vinodkumar, R.; Rajan, G.; Gopchandran, K.G.; Mahadevan Pillai, V.P. Structural, optical, and morphological properties of laser ablated ZnO doped Ta_2O_5 films. *Mater. Sci. Eng. B* **2010**, *174*, 150–158. [CrossRef]
32. Chen, X.; Bai, R.; Huang, M. Optical properties of amorphous Ta_2O_5 thin films deposited by RF magnetron sputtering. *Opt. Mater.* **2019**, *97*, 109404. [CrossRef]
33. Băilă, D.-I.; Vițelaru, C.; Trușcă, R.; Constantin, L.R.; Păcurar, A.; Parau, C.A.; Păcurar, R. Thin Films Deposition of Ta_2O_5 and ZnO by E-Gun Technology on Co-Cr Alloy Manufactured by Direct Metal Laser Sintering. *Materials* **2021**, *14*, 3666. [CrossRef]
34. Mihaiu, S.; Toader, A.; Atkinson, I.; Mocioiu, O.C.; Hornoiu, C.; Teodorescu, V.S.; Zaharescu, M. Advanced Ceramics in the SnO_2-ZnO Binary System. *Ceram. Int.* **2015**, *41*, 4936–4945. [CrossRef]
35. Potera, P.; Virt, I.S.; Cieniek, B. Structure and Optical Properties of Transparent Cobalt-Doped ZnO Thin Layers. *Appl. Sci.* **2023**, *13*, 2701. [CrossRef]
36. Wang, B.; Wang, X.; Li, M.; Hou, J.; Zhang, R. Study on the optical properties and electrochromic applications of LTO/TaOx ion storage-transport composite structure films. *Ionics* **2018**, *24*, 3995–4003. [CrossRef]
37. Rubio, F.; Albella, J.M.; Denis, J.; Martinez-Duart, J.M. Optical properties of reactively sputtered Ta_2O_5 films. *J. Vac. Sci. Technol.* **1982**, *21*, 1043–1052. [CrossRef]
38. Makuła, P.; Pacia, M.; Macyk, W. How to correctly determine the band gap energy of modified semiconductor photocatalysts based on UV–VIS spectra. *J. Phys. Chem. Lett.* **2018**, *9*, 6814–6817. [CrossRef] [PubMed]
39. Gomaa, H.M.; Yahia, I.S.; Zahran, H.Y. Correlation between the static refractive index and the optical bandgap: Review and new empirical approach. *Phys. B Condens. Matter* **2021**, *620*, 413246. [CrossRef]

40. Ravindra, N.M.; Auluck, S.; Srivastava, V.K. On the Penn Gap in Semiconductors. *Phys. Stat. Sol.* **1979**, *93*, K155. [CrossRef]
41. Mocioiu, O.C.; Vladut, C.M.; Atkinson, I.; Bratan, V.; Mocioiu, A.-M. The Influence of Gel Preparation and Thermal Treatment on the Optical Properties of SiO_2-ZnO Powders Obtained by Sol–Gel Method. *Gels* **2022**, *8*, 498. [CrossRef] [PubMed]